Interlayer locking and atomic-scale friction in commensurate small-diameter boron nitride nanotubes

Shin, Homin; Kim, Keun Su; Simard, Benoit; Klug, Dennis D.

Publisher's version / Version de l'éditeur:
https://doi.org/10.1103/PhysRevB.95.085406
Physical Review B, 95, 8, 2017-02-06

Interlayer locking and atomic-scale friction in commensurate small-diameter boron nitride nanotubes

Homin Shin,* Keun Su Kim, Benoit Simard, and Dennis D. Klug
Security and Disruptive Technologies Portfolio, Emerging Technologies Division, National Research Council Canada, Ottawa, Ontario, Canada K1A 0R6

(Received 13 November 2016; published 6 February 2017)

Density functional theory applied to small-diameter boron nitride nanotubes (BNNTs) finds out-of-plane structural *buckling* in contrast to large-diameter tubes that exhibit *faceting*. Buckling significantly affects interlayer interactions in commensurate double-walled BNNTs. Energy corrugation amplitudes in relative motions of BNNT walls change up to fourfold, depending on interlayer registry relaxation, in marked contrast to carbon nanotubes. Large differences between *relaxed* and *unrelaxed* energy corrugations of BNNTs could yield energy dissipation via the strain-induced anelastic relaxation of interlayer locking (or "lattice kinks"), which can be exploited for mechanical damping applications.

DOI: 10.1103/PhysRevB.95.085406

Understanding the interlayer mechanics of van der Waals (vdW) bonded materials is of critical importance in exploring a wide range of their applications, from fabricating superlubric surfaces in nanoelectromechanical systems (NEMS) to nanocomposites with high mechanical damping. The nature of the constituents of the surfaces greatly dictates the interlayer interaction. While both two-dimensional (2D) graphene and hexagonal boron nitride (*h*-BN) sheets are widely used as solid lubricants [1–3], one-dimensional (1D) multiwalled boron nitride nanotubes (BNNTs) consisting of multiple concentric layers of *h*-BN were shown to possess ultrahigh interlayer sliding friction [4] and torsional stiffness [5], which contrasts markedly with their carbon counterparts; the friction between two interacting incommensurate crystalline layers almost vanishes for multiwalled carbon nanotubes (CNTs) [6–8]. For the development of durable nanodevices or ultrahigh strength nanocomposites utilizing such vdW materials, it is crucial to elucidate the roles of the highly confined geometry and chemical specificity of the constituent atoms on their interlayer sliding mechanism.

Both CNTs and BNNTs are appealing candidates for NEMS and nanoengineered composites. Considering their similar crystallographic structures, the observed high interlayer friction of BNNTs is intriguing and raised an open question on their origins. The complex interplay between electrostatic interactions and vdW forces in determining the interlayer potentials has been extensively studied for planar *h*-BN and graphene, yet not much for their one-dimensionally confined structures [9–14]. These studies showed that the atomic-scale details, such as the relatively high ionicity of BN bonds, have not offered pronounced contrasts between sliding energy profiles of *h*-BN and graphene [11]. The vastly different shear and torsional frictions between multiwalled BNNTs and CNTs can originate from subtle differences in the tube structure and morphology, such as circumferential *faceting* in the tube cross section [5], which occurs when the tube diameters are sufficiently large, typically above 5 nm. Very recently, Leven *et al.* theoretically showed that the faceting occurred more abundantly in BNNTs as compared with CNTs, which was explained by their promoted interwall chiral angle correlation due to electrostatic interactions in the BN system [15]. In such a limit of large-diameter BNNTs employed, this faceted nature could well rationalize the observed ultrahigh frictions or torsional stiffness; however, there still remains an open question as to the interlayer mechanics of the other limit of nonfaceted, small-diameter BNNTs (<5 nm) which have yet to be studied extensively, either by theory or experiment. Recent advances in the synthesis of small-diameter BNNTs also make this question far more intriguing than ever before [16–18].

In this paper, we investigate the mechanism of strong mechanical couplings through atomic lattice interlocking between concentric layers of commensurate, small-diameter double-walled BNNTs (DWBNNTs), which greatly elevates the threshold forces and internal friction with respect to the relative motion of the walls. Introducing a tight constraint on the BNNT circumference to form a small-diameter tube results in the tube lattice *buckling* of its minimum energy structure [19,20], in which B atoms locate slightly inward whereas N atoms shift outward from the tube axis, respectively. The resultant structure forms a dipolar shell with the inner cylinder positively charged and the outer one negatively charged, as illustrated in Fig. 1(a). This is owing to the slightly asymmetric hybridization between two different atomic species in the curved *h*-BN lattice; B atoms with vacant orbitals prefer to maintain the planar sp^2 hybridization while N atoms with a lone electron pair tend to adopt the sp^3 bond geometry. Such buckling effects are inversely proportional to the tube radius and often impart exotic properties to small-diameter BNNTs [21,22].

Here, we show using van der Waals (vdW) parametrized density functional theory (DFT) that the interaction between the *buckled* lattices of DWBNNTs gives rise to strong interlayer locking between two concentric walls. We consider both *relaxed* and *unrelaxed* energy corrugations of the interlayer potentials: The former represent interlayer sliding and rotation slow enough to allow a full structural relaxation (i.e., quasistatic), whereas in the latter the wall motions are fast enough to preserve any internal structures developed by interlayer interactions, not allowing the associated strains to be relaxed. We observe that upon structural relaxation there are drastic contrasts in the energy landscapes of DWBNNTs, mainly due

*Homin.Shin@nrc-cnrc.gc.ca

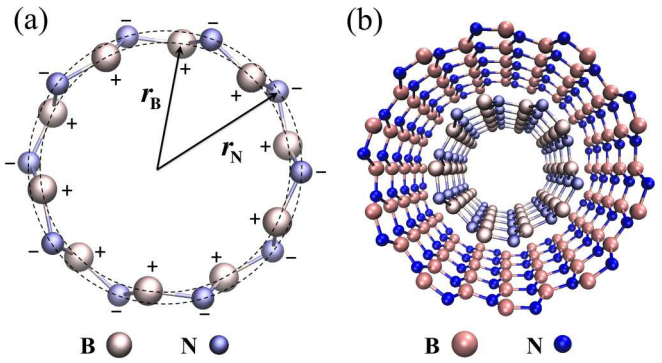

FIG. 1. Schematic top views of the equilibrium structure of a (5,5) BNNT forming a dipolar shell structure (a unit cell) (a) and the concentric double-walled (5,5)@(10,10) BNNT (b). The buckling distance, $r_N - r_B$, is estimated as 0.063 Å for the (5,5) BNNT, where r_N (r_B) is the mean radius of the N (B) atoms.

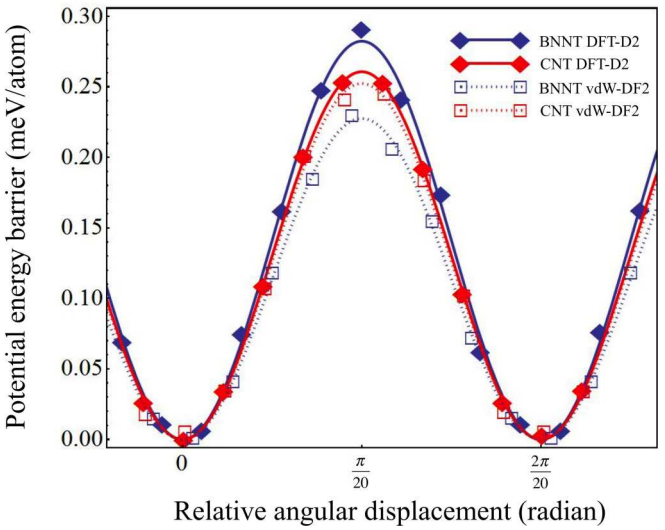

FIG. 2. Calculated rotational energy barriers upon structural relaxation of the (5,5)@(10,10) DWCNT and DWBNNT with respect to the relative angle ϕ between two concentric layers. The results from both vdW-DF2 and DFT-D2 are presented.

to the accumulated strains associated with the strong interlayer locking or "lattice kinks"; however, the graphitic interwall interaction has negligible effects on the relaxed structure of double-walled CNTs (DWCNTs) with two contacting surfaces remaining atomically smooth, which also agrees with other previous studies [6,23].

DFT calculations are performed using the Vienna *ab initio* simulation package (VASP) with the nonlocal vdW-DF2 functional [24–26]. State-of-the-art density functionals have been employed to correctly describe vdW forces in the layered *h*-BN and C systems, though the adequacy of those results is rather contradictory. Using the vdW-DF2 approach, the recent calculations on the most stable stacking modes and their energy differences for bilayer *h*-BN were shown to be in close agreement with those obtained by the high-level *ab initio* method of local second-order Møller-Plesset perturbation theory (LMP2) [10,14]. We note that slight quantitative inaccuracies among different functionals would not significantly affect the main findings of this study. The same qualitative results are also confirmed by our DFT calculation employing the empirical dispersion correction (DFT-D2) [27].

We present a comparative study of the BN and C systems by using a model coaxial (5,5)@(10,10) double-walled nanotube (DWNT) as shown in Fig. 1(b). The initial tube geometry is constructed of two concentric cylindrical hexagonal lattices with constant bond lengths (i.e., 1.45 Å for BNNTs and 1.42 Å for CNTs). The two walls are axially commensurate with the same translational periodicity a. The individual (5,5) and (10,10) tubes have $\mathbf{T}^1_{10}\mathbf{D}_{5h}$ and $\mathbf{T}^1_{20}\mathbf{D}_{10h}$ line group symmetries, respectively, and the "in-registry" orientation (i.e., the highest symmetry) state between the walls shows the rotational periodicity, $\delta_\phi = \frac{\pi}{10}$, owing to the $\mathbf{T}^1_c\mathbf{S}_{10}$ symmetry of the (5,5)@(10,10) DWNT [28]. The shifts of stacking registries are performed by translating and rotating the outer wall with respect to the inner wall, in which the different stacking positions are denoted by the coordinates of (ϕ,z), where ϕ is the angle of relative rotation of the walls about the tube axis and z is the relative displacement of the walls along the tube axis.

We first investigate the quasistatic case where one wall moves infinitesimally slowly relative to the other wall, allowing a full structural relaxation, and plot the rotational energy corrugations so obtained in Fig. 2. The results are well fitted with $U(\phi) - U_0 = \frac{\Delta U_\phi}{2}[1 - \cos(\frac{2\pi}{\delta_\phi}\phi)]$, where $U(\phi)$ is the total interaction potential, U_0 the potential energy of the ground energy stacking order, and ΔU_ϕ the rotational energy barriers. The 2D energy maps as a function of (ϕ,z) are also plotted in Figs. 3(a) and 3(d) for the BN and C systems, respectively, both of which are found to preserve the same periodicities ($\delta_\phi = \frac{\pi}{10}$, $\delta_z = a/2$) of the energy map pattern calculated on the basis of harmonics invariant under the symmetry of the (5,5)@(10,10) DWNT [23]. Thus, in such a quasistatic process, the intrinsic geometry of the DWNT governs the overall behavior of the energy corrugation. However, the amplitudes of relaxed energy corrugation differ slightly between the two systems; the energy barrier to the relative rotation differs by only ∼5%, while that to the wall sliding is estimated to be 4.5-fold stronger for the BNNT compared to the CNT, implying that the electrostatic effect resulting from buckling is more pronounced for the sliding than for the rotation of DWBNNT. In comparison, very similar energy barriers were found for bilayer *h*-BN and graphene along the same sliding pathways [11]. Our results on the energy barriers of the (5,5)@(10,10) CNT are found to be in close agreement with the results in Ref. [29], which were calculated using the nonlocal vdW functional by Dion *et al.* [30]. The results of the rotational barrier of (5,5)@(10,10) BNNT using the Perdew-Burke-Ernzerhof (PBE/6-13G**) level of theory without geometry optimization (i.e., with constant BN bond lengths) in Ref. [12] are comparable to ours, while the translational motion was found to be frictionless with almost zero energy barrier.

In Fig. 3, we also present the lattice registries of the (5,5) and (10,10) tubes at the four critical points in the energy maps [i.e., $(\phi,z) = (0,0)$, $(\frac{\pi}{20},0)$, $(0,\frac{a}{4})$, and $(\frac{\pi}{20},\frac{a}{4})$], which are constructed by unrolling the (5,5)@(10,10) DWNT onto a plane and compressing the circumference of the (10,10)

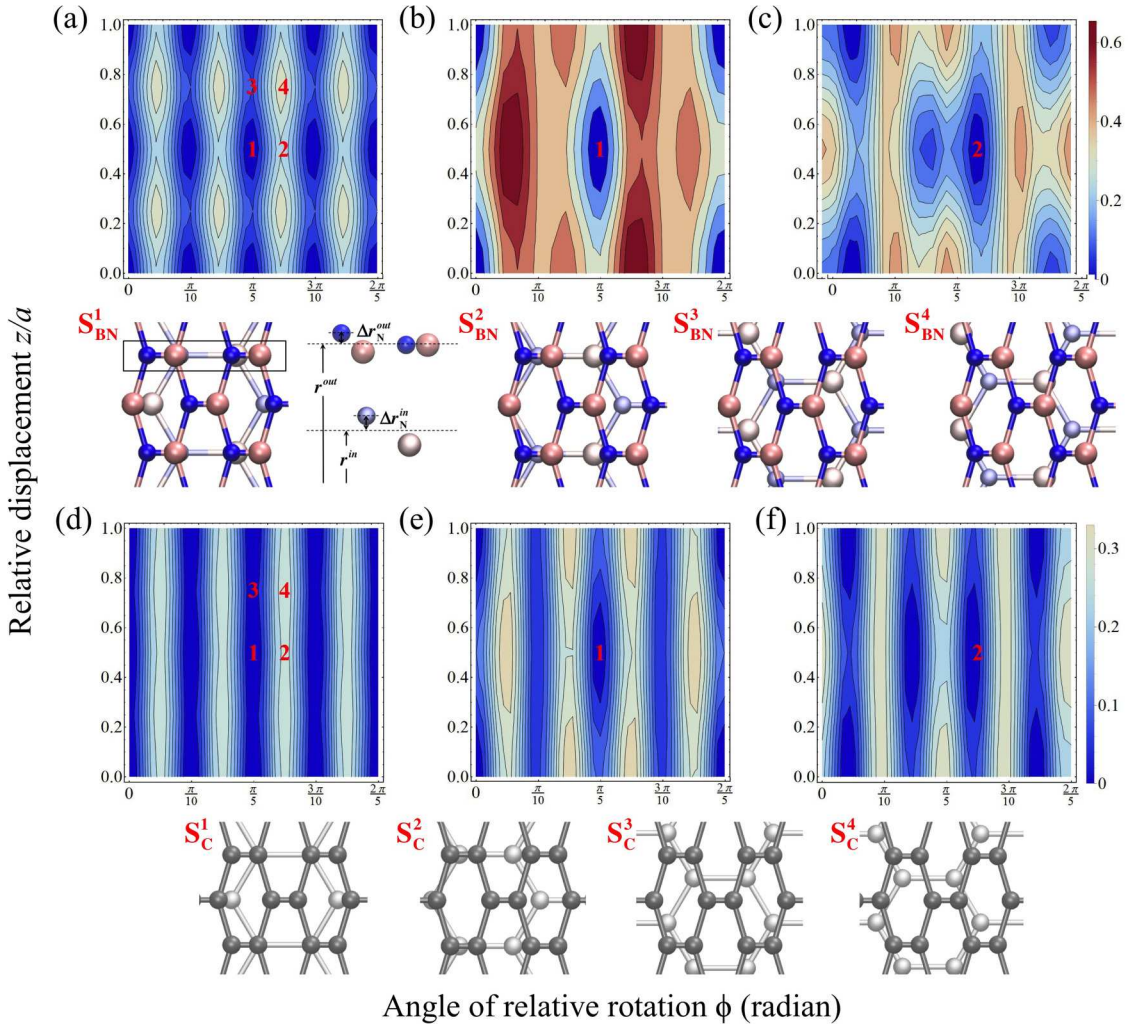

FIG. 3. The rotation-translation energy barrier maps of (a) and (d) are calculated by full structural relaxation of the (5,5)@(10,10) DWBNNT and DWCNT, respectively. The lattice registries between the (5,5) and (10,10) tubes at the different critical locations (e.g., denoted by S^1_{BN}, meaning the stacking configuration at the location 1 for the BN system) are projected into a plane as presented. For S^1_{BN}, the lateral view of a row with eclipsed B and N atoms is also displayed, where r^{in} and r^{out} refer to the average inner and outer tube radii and Δr^{in}_N is the buckling magnitude as denoted. The energy maps with respect to the stacking mode S^1_{BN}, S^2_{BN}, S^1_C, and S^2_C without structural relaxation are presented in (b), (c), (e), and (f), respectively.

tube by a scale factor of two radii. The ground state stacking configuration denoted by S^1_{BN} for the BN system is in registry with the highest symmetry maximizing the number of *eclipsed* B and N atoms. Unlike the planar case of bilayer graphene (i.e., AB stacking) or h-BN sheet (i.e., AA' stacking), the most stable configuration of S^1_C for DWCNT is the same as that of DWBNNT [31], in which the stacking modes are a combination of both the staggered and eclipsed configurations.

We now calculate the *unrelaxed* energy corrugation by rigidly sliding and rotating the outer wall of (5,5)@(10,10) DWNT, whose bond coordinates are fixed to the optimum interlayer locking configurations at the extrema in the energy maps [Figs. 3(a) and 3(d)], namely, S^1_{BN} and S^2_{BN} for DWBNNT and S^1_C and S^2_C for DWCNT. We first examine the potential energy landscape starting from the ground state stacking mode of S^1_{BN}, which is plotted in Fig. 3(b). A remarkable change from the *relaxed* energy map in Fig. 3(a) is observed; the degeneracy of the minimum energy states is lifted by reducing from a 20-fold to a fivefold rotational symmetry and the translational periodicity from $a/2$ to a, in which the DWBNNT strongly locks into the lowest-energy mode of S^1_{BN}. This interlattice locking leads to threefold and fourfold increases in the maximum energy barriers to the relative rotation (ΔU^{max}_{ϕ}) and sliding (ΔU^{max}_{z}), respectively, compared to those obtained by full relaxation (see Table I). As we will discuss below, such large energy barriers arise from the strain energy associated with the atomistic locking deformation developed through the out-of-plane degrees of freedom. The lateral view of a row with eclipsed B and N atoms of S^1_{BN} in Fig. 3 shows that the buckling of a N atom in the (10,10) tube facing a B atom in the (5,5) tube is suppressed as a result of the interactions between two buckled walls, and thereby "lattice kinks" are formed. The interlayer locking structure optimized at S^2_{BN} is also used to calculate the energy map as shown in Fig. 3(c). The DWBNNT locks into the S^2_{BN} mode, but more moderately, in which the maximum rotational and translational

TABLE I. Maximum rotational ($\Delta U_\phi^{\max}$) and translational ($\Delta U_z^{\max}$) potential energy barriers (in meV per atom) estimated from the relaxed and unrelaxed energy maps in Figs. 3(a)–3(f) for the (5,5)@(10,10) DWBNNT and DWCNT.

	$\Delta U_\phi^{\max}$	$\Delta U_z^{\max}$
BNNT full relaxation	0.229	0.068
BNNT stacking $S_{\rm BN}^1$	0.654	0.272
BNNT stacking $S_{\rm BN}^2$	0.416	0.273
CNT full relaxation	0.241	0.015
CNT stacking $S_{\rm C}^1$	0.328	0.098
CNT stacking $S_{\rm C}^2$	0.293	0.077

energy barriers are found to be twofold and fourfold increased, respectively (Table I).

For the case of the DWCNT, however, there is no significant change from the fully relaxed one, as shown in the energy maps of Figs. 3(e) and 3(f), which are constructed with $S_{\rm C}^1$ and $S_{\rm C}^2$ modes, respectively. This suggests that for the DWCNT no internal structure such as interlayer locking has been developed upon the interlayer interaction, and hence the shape of its potential energy surface has not been greatly altered in the unrelaxed case. This observation validates and agrees with other previous studies of C-based materials where mostly rigid translation and rotation were considered [6,23].

The unrelaxed energy corrugation calculated by the rigid shifts is composed of two energy contributions: The interlayer potential energy originates from the intrinsic DWNT registry symmetry, and the strain energy is associated with the lattice interlocking deformation. Since the former is obtainable from the relaxed energy corrugation, the latter strain contribution can be estimated by subtracting the relaxed energy (ΔU^R) from the unrelaxed one (ΔU^U), such that $E(\phi,z)_{\rm strain} = \Delta U^U(\phi,z) - \Delta U^R(\phi,z)$. Figure 4 demonstrates that in order to initiate the relative rotational motion between the locked layers, the large strain-induced energy barrier $\Delta E(\phi,0)$ needs to be overcome for the DWBNNT compared to the DWCNT. The average stored strain energies over 2π rotation calculated by $\varepsilon = \int^{2\pi} d\phi E(\phi,0)/2\pi$ are estimated as $\varepsilon^{\rm BNNT} = 0.258$ and $\varepsilon^{\rm CNT} = 0.055$ meV/atom.

Internal atomic distortion (i.e., "lattice kinks") developed through the buckled wall interaction in the DWBNNT would require a time-dependent relaxation in response to the relative wall motion through the self-adjustment of B and N atoms to migrate to their new equilibrium position. This manifests the *anelastic* behavior with recovering the equilibrium configuration after a finite time, and thereby dissipating mechanical

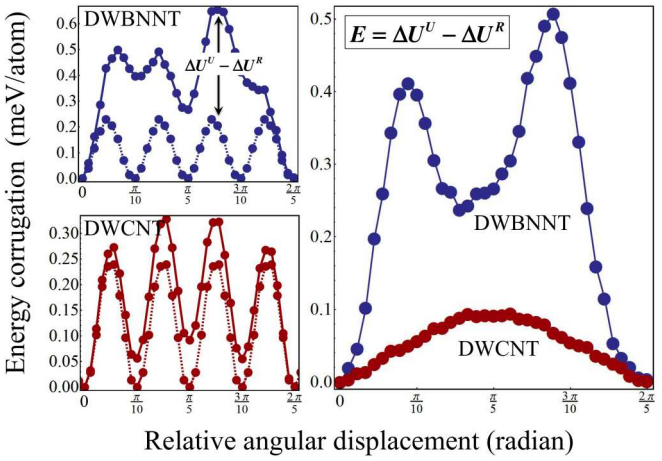

FIG. 4. The unrelaxed (ΔU^U) and relaxed (ΔU^R) rotational energy corrugations for DWBNNT (blue) and DWCNT (red) and their energy difference $E(\phi,0)_{\rm strain} = \Delta U^U(\phi,0) - \Delta U^R(\phi,0)$ are plotted.

energy by internal friction, as often observed from the point-defect or dislocation relaxation in anelastic solids [32,33]. We emphasize that we disentangle and quantify the estimates of the different source of anelastic dissipation (stored strain energy ε) from the well-known stick-slip dissipation [34]. Our calculation clearly shows that, unlike for CNTs, anelastic relaxation could be the major source of mechanical energy dissipation in the case of BNNTs, and thus the experimentally observed ultrahigh frictional drag of BNNTs is attributed to the strain-induced internal structural changes upon the wall motion.

In conclusion, our vdW modified DFT calculations identify the atomistic structural origin that gives rise to the strong interlayer locking and large energy corrugation by characterizing in detail important differences between nanotubes of different compositions. We also propose that a large amount of accumulated strain energy in buckled DWBNNTs can be dissipated via anelastic relaxation through migration of the "lattice kinks" upon rotation or sliding. There is expected to be a crossover transition in the dynamical and viscoelastic properties between the small-diameter multiwalled nanotubes where *buckling* occurs as described here and large-diameter nanotubes where *faceting* is predicted [15], which will be critical for exploiting nanotube properties on demand [35]. Anelastic interlayer mechanics can also provide insights to design different tribological properties of other vdW layered heterostructures.

This work was supported by National Research Council Canada Security Materials Technology Program.

[1] J. C. Spear, B. W. Ewers, and J. D. Batteas, Nano Today **10**, 301 (2015).
[2] C. Lee, Q. Li, W. Kalb, X.-Z. Liu, H. Berger, R. W. Carpick, and J. Hone, Science **328**, 76 (2010).
[3] M. Dienwiebel, G. S. Verhoeven, N. Pradeep, J. W. M. Frenken, J. A. Heimberg, and H. W. Zandbergen, Phys. Rev. Lett. **92**, 126101 (2004).
[4] A. Nigues, A. Siria, P. Vincent, P. Poncharal, and L. Bocquet, Nat. Mater. **13**, 688 (2014).
[5] J. Carel, I. Leven, C. Zhi, K. S. Nagapriya, R. Popovitz-Biro, D. Golberg, T. Bando, O. Hod, and E. Joselevich, Nano Lett. **12**, 6347 (2012).
[6] A. N. Kolmogorov and V. H. Crespi, Phys. Rev. Lett. **85**, 4727 (2000).

[7] J. Cumings and A. Zettl, Science **289**, 602 (2000).
[8] R. Zhang, Z. Ning, Y. Zhang, Q. Zheng, Q. Chen, H. Xie, Q. Zhang, W. Qian, and F. Wei, Nat. Nanotechnol. **8**, 912 (2013).
[9] N. Marom, J. Bernstein, J. Garel, A. Tkatchenko, E. Joselevich, L. Kronik, and O. Hod, Phys. Rev. Lett. **105**, 046801 (2010).
[10] G. Constantinescu, A. Kuc, and T. Heine, Phys. Rev. Lett. **111**, 036104 (2013).
[11] W. Gao and A. Tkatchenko, Phys. Rev. Lett. **114**, 096101 (2015).
[12] O. Hod, ChemPhysChem **14**, 2376 (2013).
[13] I. Leven, I. Azuri, L. Kronik, and O. Hod, J. Chem. Phys. **140**, 104106 (2014).
[14] A. V. Levedev, I. V. Lebedeva, A. A. Knizhnik, and A. M. Popov, RSC Adv. **6**, 6423 (2016).
[15] I. Leven, R. Guerra, A. Vanossi, E. Tosatti, and O. Hod, Nat. Nanotechnol. **11**, 1082 (2016).
[16] M. W. Smith, K. C. Jordon, C. Park, J.-W. Kim, P. T. Lillehei, R. Crooks, and J. S. Harrison, Nanotechnology **20**, 505604 (2009).
[17] K. S. Kim, C. T. Kingston, A. Hrdina, M. B. Jakubinek, J. Guan, M. Plunkett, and B. Simard, ACS Nano **8**, 6211 (2014).
[18] A. Fathalizadeh, T. Pham, W. Mickelson, and A. Zettl, Nano Lett. **14**, 4881 (2014).
[19] X. Blase, A. Rubio, S. G. Louie, and M. L. Cohen, Europhys. Lett. **28**, 335 (1994).
[20] L. Wirtz, A. Rubio, R. A. de la Concha, and A. Loiseau, Phys. Rev. B **68**, 045425 (2003).
[21] H. J. Xiang, J. Yang, J. G. Hou, and Q. Zhu, Phys. Rev. B **68**, 035427 (2003).
[22] Z. Zhang, W. Guo, and Y. Dai, J. Appl. Phys. **105**, 084312 (2009).
[23] A. V. Belikov, Y. E. Lozovik, A. G. Nikolaev, and A. M. Popov, Chem. Phys. Lett. **385**, 72 (2004).
[24] G. Kresse and J. Furthmuller, Phys. Rev. B **54**, 11169 (1996).
[25] K. Lee, E. D. Murray, L. Kong, B. I. Lundqvist, and D. C. Langreth, Phys. Rev. B **82**, 081101 (2010).
[26] The basis set consists of plane waves with a cutoff energy of 600 eV and the projector-augmented-wave (PAW) methods with the frozen core approximation are used. The supercell dimensions are $24 \times 24 \times 2.46$ Å^3 and $24 \times 24 \times 2.50$ Å^3 for CNTs and BNNTs, which contain $N = 60$ atoms/cell. The integration over the Brillouin zone was performed using the Monkhorst-Pack method with a $1 \times 1 \times 30$ k-point grid. The geometrically optimized configurations of DWNTs are obtained by relaxing all the atomic coordinates using the conjugated gradient algorithm, until the residual force became less than 0.01 eV/Å. In all the calculations, periodic boundary conditions are imposed along the tube axis to simulate infinitely long DWNTs, thus the effects of tube edges and contact area were not considered.
[27] S. Grimme, J. Comput. Chem. **27**, 1787 (2006).
[28] M. Damnjanovic, I. Milosevic, T. Vukovic, and R. Sredanovic, Phys. Rev. B **60**, 2728 (1999).
[29] G. Roman-Perez and J. M. Soler, Phys. Rev. Lett. **103**, 096102 (2009).
[30] M. Dion, H. Rydberg, E. Schroder, D. C. Langreth, and B. I. Lundqvist, Phys. Rev. Lett. **92**, 246401 (2004).
[31] J.-C. Charlier and J.-P. Michenaud, Phys. Rev. Lett. **70**, 1858 (1993).
[32] A. S. Nowick and B. S. Berry, *Anelastic Relaxation in Crystalline Solids* (Academic, New York, 1972).
[33] G. Cheng, C. Miao, Q. Qin, J. Li, F. Xu, H. Haftbaradaran, E. C. Dickey, H. Gao, and Y. Zhu, Nat. Nanotechnol. **10**, 687 (2015).
[34] A. Vanossi, N. Manini, M. Urbakh, S. Zapperi, and E. Tosatti, Rev. Mod. Phys. **85**, 529 (2013).
[35] N. Ares, T. Pei, A. Mavalankar, M. Mergenthaler, J. H. Warner, G. A. D. Briggs, and E. A. Laird, Phys. Rev. Lett. **117**, 170801 (2016).